Role of Glu312 in Binding and Positioning of the Substrate for the Hydride Transfer Reaction in Choline Oxidase[†,‡]

Osbourne Quaye,[§,||] George T. Lountos,[||,⊥,◆] Fan Fan,[+,@] Allen M. Orville,[*,⊥,#] and Giovanni Gadda[*,§,+,○]

Departments of Chemistry and Biology and The Center for Biotechnology and Drug Design, Georgia State University, Atlanta, Georgia 30302-4098, and School of Chemistry and Biochemistry and Parker Petit Institute for Bioengineering and Bioscience, Georgia Institute of Technology, Atlanta, Georgia 30332-0400

Received August 31, 2007; Revised Manuscript Received November 2, 2007

ABSTRACT: Choline oxidase catalyzes the oxidation of choline to glycine betaine, a compatible solute that accumulates in pathogenic bacteria and plants so they can withstand osmotic and temperature stresses. The crystal structure of choline oxidase was determined and refined to a resolution of 1.86 Å with data collected at 100 K using synchrotron X-ray radiation. The structure reveals a covalent linkage between His99 Nϵ2 and FAD C8M atoms, and a 123 Å^3 solvent-excluded cavity adjacent to the *re* face of the flavin. A hypothetical model for choline docked into the cavity suggests that several aromatic residues and Glu312 may orient the cationic substrate for efficient catalysis. The role of the negative charge on Glu312 was investigated by engineering variant enzymes in which Glu312 was replaced with alanine, glutamine, or aspartate. The Glu312Ala enzyme was inactive. The Glu312Gln enzyme exhibited a K_d value for choline at least 500 times larger than that of the wild-type enzyme. The Glu312Asp enzyme had a k_{cat}/K_{O_2} value similar to that of the wild-type enzyme but k_{cat} and k_{cat}/K_m values that were 230 and 35 times lower, respectively, than in the wild-type enzyme. These data are consistent with the spatial location of the negative charge on residue 312 being important for the oxidation of the alcohol substrate. Solvent viscosity and substrate kinetic isotope effects suggest the presence of an internal equilibrium in the Glu312Asp enzyme prior to the hydride transfer reaction. Altogether, the crystallographic and mechanistic data suggest that Glu312 is important for binding and positioning of the substrate in the active site of choline oxidase.

Choline oxidase (EC 1.1.3.17) catalyzes the two-step oxidative conversion of choline to glycine betaine with betaine aldehyde as an intermediate and molecular oxygen as the final electron acceptor (Scheme 1). This reaction is of considerable interest for biotechnological and medical reasons, due to glycine betaine accumulating to high levels in the cytoplasm of many plants and pathogenic bacteria in response to hyperosmotic and temperature stresses, ultimately resulting in the prevention of dehydration and cell death (*7*, *8*). Thus, the study of choline oxidase has potential in engineering drought resistance in economically relevant plants (*9*−*13*) and in developing therapeutic agents targeted at the inhibition of glycine betaine biosynthesis (*14*, *15*). From a fundamental standpoint, choline oxidase serves as a model system for investigating the mechanism of alcohol oxidation catalyzed by flavin-dependent enzymes primarily because the chemical step in which the substrate C−H bond is cleaved is not masked by other kinetic steps occurring in catalysis (*16*).

The elucidation at a molecular level of the catalytic mechanism of choline oxidase has been obtained from biochemical (*17*−*19*), mechanistic (*6*, *17*, *20*−*22*), and mutagenesis (*23*, *24*) studies. As schematically illustrated in Scheme 2, after the initial formation of an enzyme−choline complex, catalysis is initiated by the abstraction of the hydroxyl proton of the alcohol substrate by an as yet unidentified active site group with a pK_a of ∼7.5. The

[†] This work was supported in part by a National Science Foundation CAREER Award (MCB-0545712) and a grant from the American Chemical Society Petroleum Research Fund (37351-G4) to G.G.; by funds from the Georgia Tech Research Corp., the Georgia Institute of Technology Office of the Vice Provost for Research, a grant from the American Chemical Society Petroleum Research Fund (40310-G4), an American Heart Association Grant in Aid (0555286B), and a grant from the National Center for Research Resources (2 P41 RR012408) of the National Institutes of Health and from the Offices of Biological and Environmental Research of the U.S. Department of Energy to A.M.O.; by a Molecular Basis Disease Fellowship from Georgia State University to F.F.; and by a U.S. Department of Education GAANN Fellowship to G.T.L.

[‡] The atomic coordinates and structure factors have been deposited in the Protein Data Bank as entry 2jbv.

* To whom correspondence should be addressed. G.G.: Department of Chemistry, Georgia State University, P.O. Box 4098, Atlanta, GA 30302-4098; phone, (404) 413-5537; fax, (404) 413-5551; e-mail, ggadda@gsu.edu. A.M.O.: Biology Department, Brookhaven National Laboratory, Upton, NY 11973-5000; phone, (631) 344-4739; fax, (631) 344-2741; e-mail, amorv@bnl.gov.

[§] Department of Chemistry, Georgia State University.

[||] These authors contributed equally to this study.

[⊥] Georgia Institute of Technology.

[◆] Current address: Macromolecular Crystallography Laboratory, Center for Cancer Research, National Cancer Institute at Frederick, Frederick, MD 21702.

[@] Current address: Biochemistry Department, Albert Einstein School of Medicine, Bronx, NY 10461.

[#] Current address: Biology Department, Brookhaven National Laboratory, Upton, NY 11973-5000.

[+] Department of Biology, Georgia State University.

[○] The Center for Biotechnology and Drug Design, Georgia State University.

10.1021/bi7017943 CCC: $40.75
Published on Web 12/12/2007

Scheme 1: Two-Step, Four-Electron Oxidation Reaction of Choline Catalyzed by Choline Oxidase

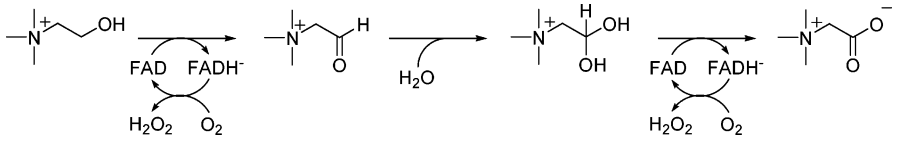

resulting choline alkoxide species is transiently stabilized in the active site of the enzyme through electrostatic interaction with the positively charged side chain of His466 (*23*, *24*). This interaction likely contributes to the preorganization of the enzyme−substrate complex that is required for the subsequent hydride transfer reaction from the α-carbon of the activated substrate to the N5 atom of the flavin cofactor. The hydride transfer reaction then occurs from the activated alkoxide species quantum mechanically via exploitation of the environmental vibrations of the reaction coordinate that permit a tunneling distance between the hydride donor and acceptor in the preorganized Michaelis complex (*21*, *25*, *26*). Preorganization of the substrate−enzyme complex likely requires the electrostatic interaction of the trimethylammonium moiety of the alcohol substrate with at least one residue in the active site of the enzyme, as suggested by mechanistic studies using an isosteric analogue of choline devoid of positive charge (*19*, *22*). However, in the absence of structural information, the identity of the amino acid residue that interacts with the positive charge of choline remains elusive.

In this study, we have initially used X-ray crystallography to gain information about the active site and the residues that form the substrate-binding cavity in choline oxidase. The structural information is complemented with mechanistic studies on enzyme variants in which the negative charge at position 312 in the active site of the enzyme was either removed by engineering mutant enzymes containing alanine or glutamine or moved away from the flavin cofactor by replacement of Glu312 with aspartate. The results of these studies demonstrate an important role for Glu312 in binding and positioning of the alcohol substrate for catalysis.

EXPERIMENTAL PROCEDURES

Materials. *Escherichia coli* strain Rosetta(DE3)pLysS was obtained from Novagen (Madison, WI). The QIAprep Spin Miniprep kit was from Qiagen (Valencia, CA). Sparse-matrix screening kits were from Hampton Research (Aliso Viejo, CA) and Nextal Biotechnologies (Montreal, QC). The QuickChange site-directed mutagenesis kit was from Stratagene (La Jolla, CA). Oligonucleotides for site-directed mutagenesis and sequencing of the mutant genes were from Sigma Genosys (The Woodlands, TX). Choline chloride was from ICN. All other reagents used were of the highest purity commercially available.

Crystallization and X-ray Data Collection. Recombinant wild-type choline oxidase from *Arthrobacter globiformis* was purified to high purity and yield and converted to the oxidized form as previously described (*19*, *27*). Crystals of choline oxidase were grown by the hanging drop vapor diffusion method, and initial crystallization conditions were obtained using commercially available sparse-matrix screening kits. Diffraction-quality crystals were obtained from 2 μL of choline oxidase (4.9 mg/mL) mixed with 2 μL of reservoir solution containing 0.1 M Bis-Tris propane (pH 8.5), 1.2 M ammonium sulfate, and 10% (v/v) dimethyl sulfoxide (DMSO) on a silanized cover slip sealed over the reservoir solution. The enzyme drops were equilibrated over 1 mL of the reservoir solution at 23 °C from which yellow rodlike crystals of oxidized enzyme grew to maximal dimensions of 0.2 mm × 0.05 mm × 0.05 mm within 2 weeks. Prior to being flash-frozen by quick submersion into liquid nitrogen, single crystals were cryoprotected by being transferred into 2 μL of 3.4 M sodium malonate (pH 7) (*28*) and allowed to incubate for 2 min at 23 °C. Two independent data sets were collected from two crystals held at approximately 100 K at the SER-CAT facilities at the Advanced Photon Source, Argonne National Laboratory (Argonne, IL). A 1.86 Å resolution data set was collected at beamline 22-ID using a 1 Å X-ray beam, a 0.2° oscillation angle, and a 2 s exposure time per frame. The data set at 2.69 Å resolution was collected at beamline 22-BM with a 1 Å X-ray beam, a 0.5° oscillation angle, and a 60 s exposure time. The diffraction images were processed with HKL2000 and scaled with SCALEPACK (*29*).

Determination of the Crystal Structure. The diffraction data from the two data sets were consistent with space group $P4_32_12$ or $P4_12_12$, with the following unit cell dimensions: $a = b = 84.4$ Å, and $c = 343.5$ Å. The Matthews coefficient (*30*, *31*) and solvent content calculations suggested two protein subunits per asymmetric unit ($V_M = 2.5$ Å^3 Da^{-1}; 50% solvent content). Molecular replacement was performed using MOLREP (*32*) from the CCP4 suite of programs (*33*) to obtain the initial phases. The search model was derived from glucose oxidase [PDB entry 1CF3 (*34*)], the sequence of which is 26% identical with that of choline oxidase with *B*-factors set at 20 Å^2. Solvent, FAD,[1] and divergent portions of the amino acid sequence were deleted from the search model, and conserved but nonidentical residues were converted to alanine residues. Cross rotation and translation searches for two molecules in the asymmetric unit were performed with data between 15 and 3.5 Å resolution in both $P4_32_12$ and $P4_12_12$ space groups. The best solution in each space group was then subjected to rigid body refinement with data from 50 to 1.86 Å resolution using CNS (*35*). Space group $P4_32_12$ gave interpretable electron density maps that were determined to be correct. The starting model had an R_{factor} of 0.48 and an R_{free} of 0.54. Phases calculated from the initial model were extracted with SIGMAA in CCP4 and were used as the starting phases in PRIME & SWITCH (*36*) as implemented in RESOLVE (*37*), which significantly improved the electron density maps. Multiple rounds of manual model rebuilding and positional and isotropic *B*-factor refinement were carried out with O (*38*) and REF-

[1] Abbreviations: CHO-E312A, choline oxidase variant in which Glu312 was replaced with Ala; CHO-E312Q, choline oxidase variant in which Glu312 was replaced with Gln; CHO-E312D, choline oxidase variant in which Glu312 was replaced with Asp; CHO-WT, wild-type choline oxidase; FAD, flavin adenine dinucleotide; GMC oxidoreductases, glucose-methanol-choline oxidoreductases.

MAC5 (*39*), respectively. Progress of the refinement was monitored by R_{free}, which was calculated using 5% of the reflections, and cross validated (σ_A-weighted $2mF_o - DF_c$ and $mF_o - DF_c$ maps) to evaluate the model and correct errors (*40*).

After several rounds of refinement and model building, the FAD was built into the electron density. Library files containing the topology and parameter files for the FAD were prepared using the Dundee PRODRG server (*41*). Planar restraints were enforced on the oxidized isoalloxazine ring of FAD for several rounds of refinement. When the overall R_{factor} decreased below 0.3, water molecules were placed with ARP/Waters (*42*), refined with REFMAC5, and manually inspected. Within each active site, a single DMSO molecule, an additive used in the crystallization solution, was fit into electron density near the N5 position of the isoalloxazine ring of the flavin and refined. For comparison, a sulfate molecule was also fit in this position and refined, but inspection showed that DMSO fit the electron density better. The electron density for the isoalloxazine of the FAD ring was not planar;[2] consequently, several rounds of σ-weighted simulated annealing composite omit refinement and their corresponding maps were examined in the final stages of the model refinement. The omitted atoms included the whole flavin, DMSO, and all residues within 6 Å of the isoalloxazine ring system. Structure validation of model geometry was carried out with PROCHECK (*43*, *44*). Solvent-exposed surface areas were calculated with a 1.4 Å probe radius with Swiss-PDB viewer (version 3.7b2) or VEGA (http://www.ddl.unimi.it). Secondary structure assignments were made using KSDSSP (*45*). Structural homologues in the Protein Data Bank were found using MSDfold (http://www.ebi.ac.uk/msd-srv/ssm/). The rms differences between models were calculated with SSM (http://www.ebi.ac.uk/msd-serv/ssm) or Swiss-PDB viewer (version 3.7b2). Figures showing structures were prepared using Swiss-PDB viewer (version 3.7b2) and PovRay (version 3.5) or Pymol (DeLano Scientific LLC, Castro City, CA).

Site-Directed Mutagenesis. Mutant genes for choline oxidase variants CHO-E312A, CHO-E312Q, and CHO-E312D were prepared using the pET/*codA*mg plasmid for the wild-type enzyme as a template (*27*) and forward and reverse oligonucleotides as primers for site-directed mutagenesis. Site-directed mutagenesis was carried out using the QuikChange site-directed mutagenesis kit following the manufacturer's instruction manual in the presence of 2% DMSO. The resulting mutant genes (pET/*codA*mg-E312A, -E312Q, and -E312D) were sequenced at the DNA Core Facility at Georgia State University using an Applied Biosystems Big Dye Kit on an Applied Biosystems model ABI 377 DNA sequencer to confirm the presence of the mutant genes in their correct orientations. As an expression host, competent cells of *E. coli* strain Rosetta(DE3)pLysS were transformed with the mutant plasmids by electroporation, and permanent stocks of the transformed cells were prepared and stored at −80 °C.

Expression and Purification of Choline Oxidase Variants. The variant enzymes were expressed and purified to homogeneity as previously described for wild-type choline oxidase (*19*, *27*). To increase the stability of the variant enzymes during purification, 10% glycerol was incorporated in the buffers throughout the purification steps with the exception of the dialysis step at pH 6 in which the anionic semiquinone form of the enzyme was converted to the oxidized form (*19*). Enzymes stored at −20 °C in 20 mM Tris-HCl (pH 8) were found to be stable for at least 6 months.

Biochemical Studies. To ascertain that FAD was covalently bound to the proteins, we treated the purified enzymes with 10% trichloroacetic acid (TCA) after recording the spectra for the bound flavin. The enzyme/TCA mixtures were incubated for 30 min on ice and centrifuged at 20000*g* for 10 min. The UV−vis spectra of the supernatants were recorded again to check the presence of unbound FAD. All UV−visible absorbance spectra were recorded using an Agilent Technologies diode-array model HP 8453 spectrophotometer.

Kinetic Assays. Enzyme activities of CHO-E312Q and CHO-E312D were measured by the method of initial rates in 50 mM potassium phosphate or 50 mM sodium pyrophosphate as described for wild-type choline oxidase (*16*). The enzymatic activities were measured by monitoring the rate of oxygen consumption with a computer-interfaced Oxy-32 oxygen monitoring system (Hansatech Instrument) at 25 °C.

Steady-state kinetic parameters for CHO-E312D were determined at varying concentrations of choline between 0.01 and 20 mM and oxygen between 0.03 and 1.1 mM. Each reaction mixture was equilibrated at the desired oxygen concentration by bubbling the appropriate O_2/N_2 gas mixture for a minimum of 10 min. The pH profiles of the kinetic parameters with choline as a substrate for CHO-E312D were determined at the atmospheric oxygen concentration due to the low K_m values for oxygen determined at pH 5 and 10. All enzyme assays were conducted in 50 mM sodium pyrophosphate, with the exception of pH 7 where 50 mM potassium phosphate was used. Substrate kinetic isotope effects on the steady-state kinetic parameters were determined by alternating varying concentrations of the substrate isoptomers, choline and [1,2-$^2H_4$]choline, at an atmospheric concentration of oxygen. Solvent viscosity effects on steady-state kinetic parameters were measured in 50 mM sodium pyrophosphate (pH 10 and 25 °C) using glucose and sucrose as viscosigens; the relative viscosity values at 25 °C were calculated according to the reference values at 20 °C from Lide (*46*).

[2] An outstanding feature of the electron density for the FAD is that the isoalloxazine ring is not planar, as anticipated for oxidized flavin. The observed distortions also differ significantly from the structures of reduced flavins, which typically exhibit an approximately 150° angle along the N5−N10 axis defined by the dimethylbenzene and pyrimidine rings (*1*, *2*). In contrast, the dimethylbenzene and piperazine rings in choline oxidase are essentially flat and coplanar, but the plane of the pyrimidine ring is at an approximately 120° angle to the former plane. The C4a atom of FAD appears to be sp^3 hybridized, which is suggestive of a covalent adduct in the crystals. However, the aerobic crystallization materials and conditions did not include any reagent known to form a C4a adduct with FAD, with the exception of O_2. It is noteworthy that O_2 is known to react with reduced flavins at the C4a position of the isoalloxazine ring in flavin-dependent monooxygenases and possibly in flavoprotein oxidases (*3*). The crystallographic data indicate that the C4a adduct contains either one or two C, N, or O atoms. Because of this uncertainty, the flavin and adduct are listed in the PDB coordinates as FAO and UNK, respectively. The nature of the FAD C4a covalent adduct is currently under investigation using structural, spectroscopic, and computational approaches, and the results of these studies will be reported elsewhere.

Rates of flavin reduction with varying concentrations of substrate (choline or [1,2-$^2H_4$]choline), measured via rapid kinetics, were determined on a Hi-Tech SF-61 stopped-flow spectrophotometer thermostated at 25 °C in 50 mM sodium pyrophosphate (pH 10). Reduction of the oxidized enzyme-bound flavin upon mixing with substrate was monitored by a decrease in absorbance at 450 nm. The enzyme was previously made anaerobic by alternately applying vacuum and flushing with oxygen-free argon for 25 cycles and mounted onto the stopped-flow apparatus also previously treated with 0.26 mM degassed dithionite or a mixture of glucose (5 mM) and glucose oxidase (3600 units) to scrub oxygen. The substrate was flushed with oxygen-free argon for at least 15 min prior to being mounted onto the stopped-flow apparatus. Equal volumes of CHO-E312Q or CHO-E312D and substrate were mixed anaerobically in the stopped-flow apparatus, yielding a final enzyme concentration of ~20 μM.

Data Analysis. Data were fit with KaleidaGraph (Synergy Software, Reading, PA) and EnzFitter (Biosoft, Cambridge, U.K.). Stopped-flow traces were fit to eqs 1 and 2, which describe single- and double-exponential processes, respectively, where k_{obs}, k_{obs1}, and k_{obs2} represent first-order rate constants, t is time, A_t is the value of absorbance at 450 nm at any given time, A, A_1, and A_2 are the amplitudes of the absorbance changes, and A_∞ is the absorbance at infinite time. Pre-steady-state kinetic parameters were determined by using eq 3, where k_{obs} is the observed first-order rate for the reduction of the enzyme-bound flavin at any given concentration of substrate, k_{red} is the limiting first-order rate constant for flavin reduction at a saturating substrate concentration, and K_d is the dissociation constant for binding of the substrate to the enzyme. Steady-state kinetic parameters in atmospheric oxygen were determined by fitting the initial rates at different concentrations of substrate to the Michaelis−Menten equation for one substrate. Steady-state kinetic parameters at varying concentrations of choline and oxygen were determined by fitting the initial rates data to eq 4, which describes a steady-state kinetic mechanism with intersecting lines in double-reciprocal plots, where e represents the concentration of enzyme, k_{cat} is the turnover number of the enzyme at infinite substrate concentrations, and K_a and K_b represent the Michaelis constants for the organic substrate (A) and oxygen (B), respectively. The pH dependences of the steady-state kinetic parameters with choline were determined by fitting the initial rates data to eq 5, which describes a curve with a slope of 1 and a plateau region at high pH, where C is the pH-independent value of the kinetic parameter of interest. Solvent viscosity effects on the k_{cat}/K_m and k_{cat} values for choline were fit to eq 6, where $(k)_o$ and $(k)_\eta$ are the kinetic parameters of interest in the absence and presence of viscosigen, respectively, S is the degree of viscosity dependence, and η_{rel} is the relative viscosity.

$$A_t = Ae^{-k_{obs}t} + A_\infty \quad (1)$$

$$A_t = A_1e^{-k_{obs1}t} + A_2e^{-k_{obs2}t} + A_\infty \quad (2)$$

$$k_{obs} = \frac{k_{red}A}{K_d + A} \quad (3)$$

$$\frac{v}{e} = \frac{k_{cat}AB}{K_aB + K_bA + AB + K_{ia}K_b} \quad (4)$$

$$\log Y = \log\left(\frac{C}{1 + \frac{10^{-pH}}{10^{-pK_a}}}\right) \quad (5)$$

$$\frac{(k)_o}{(k)_\eta} = S(\eta_{rel} - 1) + 1 \quad (6)$$

RESULTS

Determination of the Crystal Structure. The X-ray data collection and atomic model refinement statistics are listed in Table 1. X-ray diffraction data were obtained with synchrotron radiation from two independent crystals of choline oxidase; although nearly identical structures were obtained from both data sets, one crystal diffracted to higher resolution (1.86 Å compared to 2.69 Å). That data set consists of 381 317 observations of 97 546 unique reflections in the resolution range from 50 to 1.86 Å. The structure was determined by molecular replacement with a search model based upon glucose oxidase from *Aspergillus niger* (PDB entry 1CF3) (*34*). The atomic model was refined against the 1.86 Å resolution data set to a final R_{factor} of 0.161 and an R_{free} of 0.202. An overall coordinate error of the model based on an R_{factor} of 0.13 Å was determined. The final model had a correlation coefficient of 0.967. Ramachandran analysis of the crystal structure showed that 89.4% of the residues are in the most favored region, 10% in the additionally allowed regions, 0.6% in the generously allowed regions, and 0.1% in the disallowed regions. Ala230 in the A chain was flagged as being in the disallowed region, but the electron density maps indicate this residue fits well in the observed density.

Overall Structure Description. The X-ray structure revealed that choline oxidase crystallized as a homodimer with approximate dimensions of 88 Å × 70 Å × 46 Å (Figure 1), in agreement with solution measurements showing a dimeric structure under native conditions (*27*). Each monomer contains 546 residues; however, the last 19 residues in the C-terminal portion of each monomer were not visible in the electron density maps and were not included in the final model. The two monomers in the asymmetric unit of the holoenzyme were overlaid with a rms deviation of 0.23 Å over 527 common C_α atoms. The buried surface area at the subunit interface was approximately 2430 Å^2, which corresponds to approximately 13% of the total surface area for each monomer. The dimer interface included two sets of six identical intersubunit contacts between charge complementary residues clustered on the outer edges of the interface. These are Asp72−Lys398 (4.1 Å), Asp250−Glu53 (4.3 Å), Arg255−Glu370 (3.2 Å), Asp358−Arg396 (2.4 Å), Arg363−Asp394 (4.2 Å), and Arg363−Asp397 (2.9 Å). In contrast, the central portion of the dimer interface contains very few close contacts between subunits, which include the Asp72−Lys398 contact (4.1 Å).

Table 1: X-ray Diffraction Data Collection and Model Refinement Statistics

	crystal 1	crystal 2
Diffraction Data Collection Statistics		
X-ray wavelength (Å)	1.0	1.0
resolution range (Å)	50−1.86 (1.91−1.86)[a]	50−2.69 (2.76−2.69)[a]
space group	$P4_32_12$	$P4_32_12$
unit cell dimensions (Å)		
$a = b$	84.4	84.4
c	343.5	343.7
total no. of reflections	381317	196964
no. of unique reflections	97546	33722
multiplicity	3.9 (2.8)[a]	5.8 (2.4)[a]
completeness (%)	92.3 (63.2)[a]	94.2 (69.7)[a]
R_{sym} (%)[b]	7.2 (31.5)[a]	10.8 (27.1)[a]
$I/(\sigma)I$[c]	17.7 (2.3)[a]	15.6 (2.8)[a]
Model Refinement Statistics		
resolution range (Å)	50−1.86	50−2.69
no. of reflections	92403	31943
no. of protein atoms	8171	8168
no. of water molecules	960	152
R_{factor}	0.161	0.157
R_{free}[d]	0.202	0.219
average B-factor (Å^2)		
protein	22.5	25.5
water	32.6	17.5
FAO (2)[e]	17.4	20.4
UNX (2)[f]	24.8	37.2
DMSO (2)	40.0	44.1
rms deviations from ideal		
bond lengths (Å)	0.014	0.018
bond angles (deg)	1.5	1.7
correlation coefficient	0.967	0.954
estimated coordinate error (Å)	0.128	0.219

[a] Values for the highest-resolution shell of data are given in parentheses. [b] $R_{sym}(I)$ gives the average agreement between the independently measured intensities such as $\sum_h\sum_i|I_i - I|/\sum_h\sum_i I$, where I is the mean intensity of the i observations of reflection h. [c] $I/\sigma(I)$ is the root-mean-square value of the intensity measurements divided by their estimated standard deviation. [d] Calculated with 5% of the data. [e] The flavin with the sp^3-hybridized C4a atom. [f] The unknown C4a adduct.

The protein fold of each choline oxidase subunit resembles that of other members of the glucose-methanol-choline (GMC) oxidoreductase enzyme superfamily (*5*, *34*, *47*−*55*). The structure-based sequence alignment is quantified in Table S1 and shown in Figure S1 of the Supporting Information. The two-domain topology is similar to that of glucose oxidase and the bacterial flavoenzyme *p*-hydroxybenzoate hydroxylase, with a typical PHBH fold (*56*). The FAD-binding domain is formed primarily by residues 1−159, 201−311, and 464−527 (Figure 1). This domain consists of a six-stranded parallel β-sheet that is flanked on one side by a three-stranded antiparallel β-sheet and further surrounded by eight α-helices. The substrate binding domain is formed primarily by residues 160−200 and 312−463. The topology of the substrate binding domain consists of a distorted six-stranded antiparallel β-sheet, which forms the bottom of the choline oxidase active site and is flanked on the other side by three α-helices that protrude into the bulk solvent.

A common feature of other members of the GMC family is a loop that forms a lid over the putative substrate binding site (*48*, *50*, *51*, *55*). In choline oxidase, this loop region is composed of residues 64−95 (Figure 1 and Figure S1 of the Supporting Information). The average *B*-factor of these residues is 20 Å^2, indicating that the loop is well-defined in the crystal structure. A portion of the loop is shielded from bulk solvent by the second monomer of the dimer; however, residues 74−85 extend into the bulk solvent. The loop is amphipathic with hydrophobic residues directed toward the interior and hydrophilic residues directed toward the external surface.

FAD Binding Site. The FAD isoalloxazine ring is buried within the protein so that no parts are visible from the molecular surface of the protein.[2] Solvent-accessible surface calculations indicate that only 21.5 Å^2 (2.1%) of the entire FAD surface area is exposed to the solvent. The electron density maps clearly indicate that the FAD is covalently linked to the His99 Nϵ2 atom via the FAD C8M atom of the isoalloxazine ring (Figure 2). This contrasts to previous mass spectrometric studies by other authors that proposed His87 as the residue covalently attached to FAD^{C8M} (*57*). Indeed, His87 is part of the loop that covers the active site cavity (see above) and is located approximately 7.7 Å from the FAD C8M atom.

Substrate Binding Site. Upon completion of the refinement, electron density with greater than +4.5σ positive difference features was still present approximately 4 Å from the N5 atom of the isoalloxazine ring. The shape and size of the electron density clearly indicated that this species was not a water molecule. The crystallization solution that was used contained DMSO and ammonium sulfate. Refinement of either DMSO or sulfate ion indicated that the former ligand fits well into the electron density but the latter does not. As illustrated in Figure 2, the methyl groups of DMSO project toward Val464 (3.7 Å) and His351 (3.5 Å), whereas the oxygen atom of DMSO is within hydrogen bonding distance of Ser101 Oγ (2.7 Å) and the FAD N5 atom (2.7 Å). The average refined *B*-factor for the DMSO atoms was 40.0 Å^2, which is roughly double that of the protein or the FAD (Table 1). Our steady-state kinetic analyses indicated that DMSO is a weak competitive inhibitor with respect to choline, with a K_I value of 460 ± 4 mM (F. Fan and G. Gadda, unpublished observations).

Analysis of the molecular surfaces of the protein reveals a solvent-excluded cavity with a volume of approximately 125 Å^3, located within the substrate binding domain. The cavity is adjacent to the *re* face of the FAD and is sufficiently large to accommodate a choline molecule (93 Å^3), provided that the DMSO ligand in the current structure is displaced. The cavity is partially surrounded by the hydrophobic residues Trp61, Trp331, Phe357, and Val464 (Figure 2), which form an aromatic cage. The polar residues bordering the cavity include Glu312, His351, and His466, of which the latter two are near the FAD isoalloxazine ring. Of particular importance is the side chain of Glu312, which forms the "top" of the aromatic cage and is the only negatively charged residue lining the active site cavity.

Docking of Choline into the Substrate-Binding Cavity. Earlier mechanistic studies with substrate and product analogues established that the positive charge on the trimethylammonium moiety of choline plays an important role in substrate binding and specificity in the reaction catalyzed by choline oxidase (*19*, *22*). To gain insight into the enzyme and substrate interactions, we manually docked choline into the cavity (Figure 2). The side chain of Glu312 is approximately 3 Å from the positively charged trimethylammonium moiety of choline, which suggests an ionic pair. Although other orientations are possible, in the illustrated

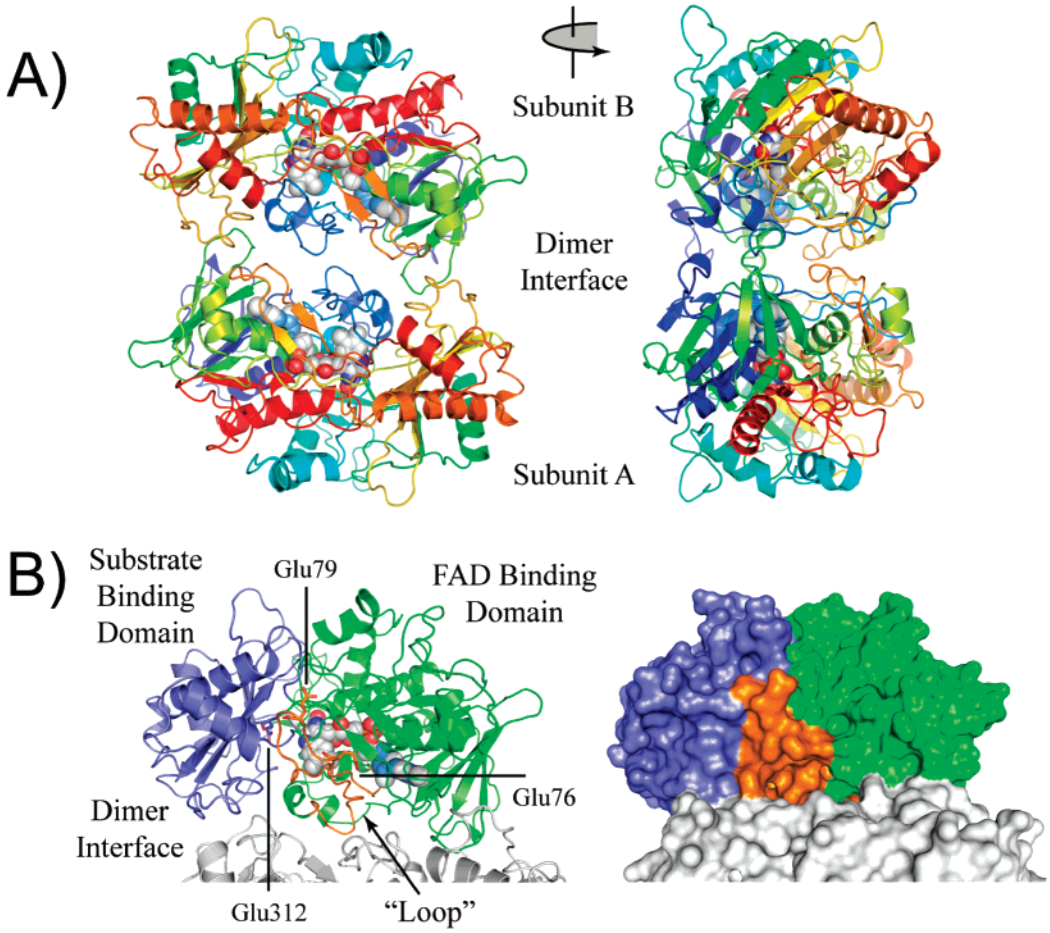

FIGURE 1: Three-dimensional structure of choline oxidase refined to 1.86 Å resolution. (A) Two orthogonal views of the choline oxidase homodimer illustrated with a cartoon ribbon trace of the protein backbone. Each subunit is colored from blue to red starting at the N-terminus. The FAD is shown as CPK atoms with the C, N, and O atoms colored gray, blue, and red, respectively. (B) A single subunit of choline oxidase illustrating the domain architecture (see the text for a discussion). The view is similar to that of panel A (left). The space-filling view is shown on the right with the surfaces colored according to the FAD binding (blue), substrate binding (green), and "loop" (orange) regions.

configuration choline appears to be poised to initiate the reductive half-reaction (i.e., oxidation of choline). For example, the choline hydroxyl O atom is approximately 4 Å from the side chains of His351, His466, and Asn512, the former two of which are good candidates for serving as active site bases. Moreover, the C1 atom of choline is less than 4 Å from the side chain of Ser101 and the flavin N5 atom, which is the locus for accepting the hydride transfer reaction.

Expression and Purification of CHO-E312A, CHO-E312Q, and CHO-E312D. Choline oxidase variants in which glutamate at position 312 was replaced with alanine, glutamine, or aspartate were expressed and purified at pH 8 in the presence of 10% glycerol, following the same protocol used for the wild-type enzyme (*27*). The addition of glycerol throughout the purification steps resulted in the increased stability of the mutant enzyme. A mixture of anionic semiquinone and oxidized flavin species were present upon isolation of the mutant enzymes (Figure S2 of the Supporting Information), which was also observed for purification of the wild-type enzyme (*19*, *27*). The fully oxidized and active enzymes used in this study were obtained by treatment at pH 6, as previously reported for the wild-type enzyme (*58*). UV−visible absorbance spectra of the supernatants after treatment of the three variant enzymes with 10% TCA and centrifugation showed no peaks around 370 and 450 nm, consistent with the flavin cofactor being covalently bound to the proteins. Thus, substitution of Glu312 with alanine, glutamine, or aspartate did not affect the covalent linkage of the flavin to the protein. There was no detectable activity for the alanine variant with up to 100 mM choline as the substrate. In contrast, the glutamine and aspartate variants were able to oxidize choline. Table 2 reports the specific activities and apparent steady-state kinetic parameters determined in atmospheric oxygen at pH 7 for the mutant enzymes.

Reductive Half-Reaction of CHO-E312Q with Choline. The involvement of the negative charge of Glu312 in binding choline was determined by directly measuring and comparing the thermodynamic equilibrium constants (K_d) with choline as the substrate for CHO-E312Q and the wild-type enzyme. Thus, the Glu312 enzyme variant was mixed anaerobically with different concentrations of choline up to 250 mM in a stopped-flow spectrophotometer at pH 10 and 25 °C, and the resulting rates of flavin reduction were measured. The high pH was chosen to avoid artifactual contributions originating from pH effects, since previous results with the wild-type enzyme (*17*, *58*), as well as CHO-E312D (this study), showed that the kinetic parameters become pH-independent at high pH. With CHO-E312Q, the observed rates of flavin reduction were hyperbolically dependent on the concentration of choline, yielding a K_d value of ≥150

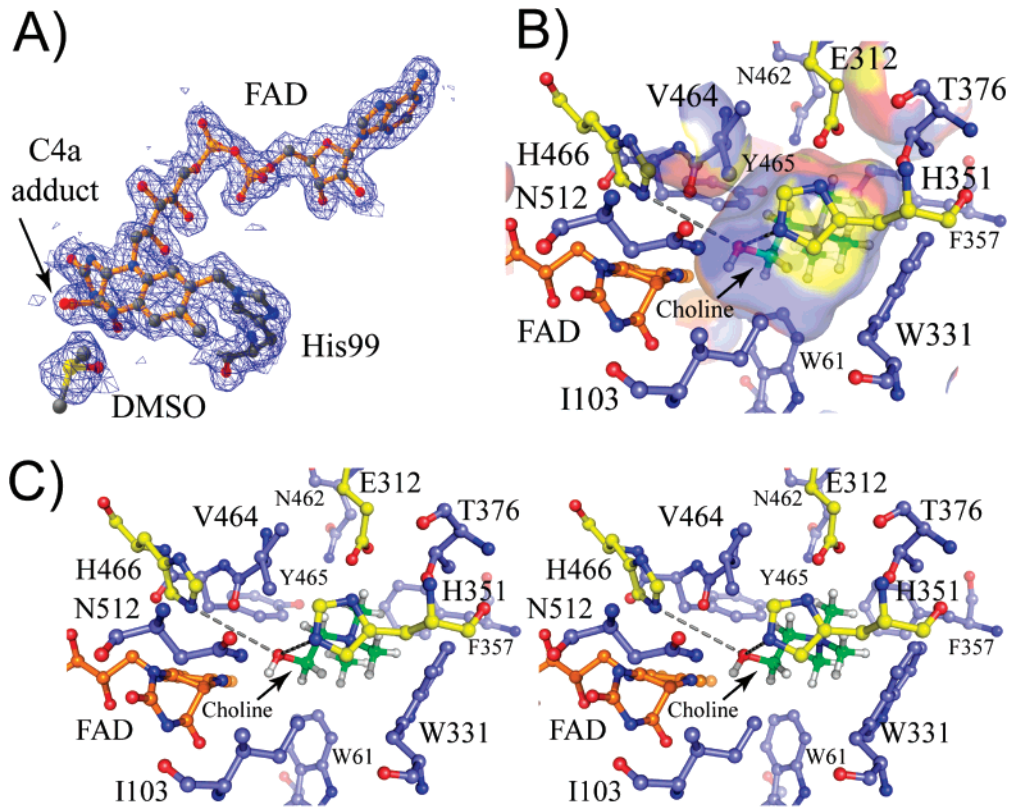

FIGURE 2: Active site of choline oxidase. (A) An example of the typical $2mF_o - DF_c$ electron density at 1.86 Å resolution (1σ contour) associated with an active site DMSO molecule, the FAD, a C4a adduct,[2] and the His99 residue. The DMSO molecule binds at the bottom of the solvent-excluded cavity and comes within 2.7 Å of the FAD N5 atom. (B) Solvent-excluded cavity illustrated with semitransparent surfaces calculated after removal of the C4a adduct and the DMSO molecule. The surfaces are colored according to the atom forming its border with generally hydrophobic and hydrophilic residues shown with their carbon atoms colored blue and yellow, respectively. The cavity volume of >120 Å^3 is sufficiently large to accommodate a choline molecule (shown with green carbon atoms). The choline molecule was manually docked into the cavity to maximize the potential interactions between the substrate and catalytically important residues such as His351, His466, FAD^{N5}, and Glu312 (see the text). The dashed lines indicate the distance between the choline oxygen atom and the Nϵ2 atoms of His351 (4.3 Å) and His466 (4.4 Å). (C) Divergent stereoview of the hypothetical choline molecule docked into the active site of choline oxidase. The view and coloring scheme are identical to that of panel B.

mM[3] (Figure S3 of the Supporting Information). This value was at least 500 times larger than the K_d value of ~0.3 mM previously reported for the wild-type enzyme under the same conditions (*16*), suggesting that the negative charge at position 312 is important for binding of the alcohol substrate in choline oxidase. Flavin reduction was followed by a slow kinetic step with a rate of ~0.01 s^{-1}, which was independent of the concentration of choline. This was tentatively assigned to the release of the product of the reaction from the reduced enzyme.

Kinetic and Mechanistic Studies with CHO-E312D. The Glu312Asp enzyme variant was investigated in an effort to establish how the spatial location of the negative charge on residue 312 in the active site of the enzyme may affect catalysis in the enzyme. The steady-state kinetic mechanism was determined at pH 10 by measuring initial rates of oxygen consumption at varying concentrations of both choline and oxygen. As for the case of the wild-type enzyme (*16*, *58*), the best fit of the data was obtained to an equation describing a sequential steady-state kinetic mechanism. As illustrated in Table 3, substitution of Glu312 with aspartate resulted in a 230-fold decrease in the k_{cat} value and a 30-fold decrease in the k_{cat}/K_m value with choline, indicating that Glu312 participates in the reductive half-reaction in which the alcohol substrate is oxidized. An upper limiting value of 2 μM could be estimated for the K_m value for oxygen from the fit of the steady-state kinetic data. Consistent with a K_m value for oxygen in the low micromolar range, the apparent rates of

Table 2: Comparison of Specific Activities and Apparent Steady-State Kinetic Parameters of CHO-E312D, CHO-E312Q, and CHO-E312A with Those of Wild-Type Choline Oxidase[a]

enzyme	total protein (mg)	specific activity (units/mg)	$^{App}k_{cat}/K_m$ (M^{-1} s^{-1})	$^{App}k_{cat}$ (s^{-1})	$^{App}K_m$ (mM)
CHO-E312D	190	0.17	1500	0.26	0.17
CHO-E312Q	104	0.013	1.8	0.21	116
CHO-E312A	120	–[b]	–	–	–
CHO-WT	220	8	25000	15	0.6

[a] Total protein amounts were determined by the Bradford method and refer to 4.5 L of liquid culture (*78*). Enzymatic activities were measured at varying concentrations of choline in the range from 0.005 to 250 mM, in 50 mM potassium phosphate (pH 7) at 25 °C, using fully oxidized enzymes. [b] No oxygen consumption was determined when 11 μM enzyme was assayed with 100 mM choline; for comparison, with the wild-type enzyme at a concentration of 0.1 μM and 10 mM choline, the rate of oxygen consumption is ~15 s^{-1}.

[3] At choline concentrations of >250 mM, inflated rates of flavin reduction in the stopped-flow spectrophotometer were observed. While such a kinetic behavior was not investigated further, an accurate determination of the K_d value for binding of choline to CHO-E312Q could not be carried out because the enzyme could not be saturated with the substrate. For this reason, only a limiting lower value of 150 mM is reported for K_d.

Table 3: Comparison of the Kinetic Parameters with Choline as the Substrate for CHO-E312D and Wild-Type Choline Oxidase at pH 10

	CHO-E312D[a]	CHO-WT[b]
k_{cat} (s^{-1})	0.26 ± 0.004	60 ± 1
k_{cat}/K_m (M^{-1} s^{-1})	7100 ± 400	237000 ± 9000
K_m (mM)	0.04 ± 0.002	0.25 ± 0.01
K_{O_2} (mM)	≤ 0.002[c]	0.69 ± 0.03
k_{cat}/K_{O_2} (M^{-1} s^{-1})	≥ 76000[d]	86400 ± 3600
k_{red} (s^{-1})	0.36 ± 0.01	93 ± 1
K_d (mM)	~ 0.1	0.29 ± 0.01
$^D k_{red}$	9.3 ± 0.2	8.9 ± 0.2
$^D(k_{cat}/K_m)$[e]	4.4 ± 1.2	10.7 ± 2.6
$^D k_{cat}$[e]	7.1 ± 1.3	7.5 ± 0.3

[a] Steady-state kinetic parameters were determined at varying concentrations of choline and oxygen in 50 mM sodium pyrophosphate (pH 10) at 25 °C. [b] Data are from ref *16*. [c] Estimated upper limiting value. [d] Estimated lower limiting value calculated from the k_{cat} value experimentally determined and the estimated upper limiting K_{O_2} value. [e] The pH-independent values are reported here.

reaction determined as a function of oxygen concentration with 10 mM choline showed that the enzyme was at least 75−80% saturated at 10 μM oxygen (Figure S4 of the Supporting Information). From the k_{cat} and K_{O_2} values, a limiting lower k_{cat}/K_{O_2} value of 76 000 could be estimated. As shown in Table 3, such a value is not significantly different from that previously determined with the wild-type enzyme, consistent with substitution of Glu312 with aspartate having a negligible effect on the oxidative half-reaction in which the enzyme-bound reduced flavin is reoxidized with formation of hydrogen peroxide.

The reductive half-reaction of CHO-E312D was investigated using a stopped-flow spectrophotometer to determine the rate of flavin reduction (k_{red}) and the K_d value for binding of choline. As for the case of the wild-type enzyme (*16*), no intermediates were observed with the enzyme undergoing a two-electron reduction to the hydroquinone state. The rate of flavin reduction was the same between 1 and 10 mM choline (Figure S5 of the Supporting Information), yielding a well-defined k_{red} value that was 260-fold lower than in the wild-type enzyme (Table 3). A K_d value of ~0.1 mM could only be estimated from the kinetic data, due to the inability to maintain pseudo-first-order conditions in the stopped-flow apparatus at choline concentrations of <50 μM. However, such a K_d value was not significantly different from that of ~0.3 mM determined previously for the wild-type enzyme, suggesting similar chemical binding affinities in choline oxidase containing glutamate or aspartate at position 312.

Substitution of choline with [1,2-$^2H_4$]choline resulted in a slower rate of flavin reduction at pH 10, yielding a $^D k_{red}$ value of 9.3 ± 0.2. This value was not significantly different from the $^D k_{red}$ value of ~9 recently reported for the wild-type enzyme (*16*), consistent with cleavage of the C−H bond of choline being rate-limiting in the reductive half-reaction.

The pH profiles of the steady-state kinetic parameters with choline as the substrate for CHO-E312D were determined in the pH range from 5 to 10 in air-saturated buffer at 25 °C, corresponding to an oxygen concentration of 250 μM. At pH 5 and 10, the K_{O_2} values were ≤ 2 μM (Figure S4 of the Supporting Information), thereby ensuring that the enzyme was saturated with oxygen throughout the pH range that was tested. As shown in Figure 3, the k_{cat}/K_m and k_{cat} values were pH-independent at high pH and decreased with

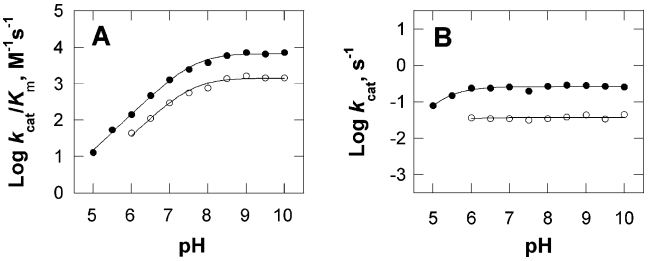

FIGURE 3: pH dependence of the k_{cat}/K_m and k_{cat} values for CHO-E312D with choline and [1,2-$^2H_4$]choline as substrates at 25 °C. (A) pH profiles for k_{cat}/K_m with choline (●) and [1,2-$^2H_4$]choline (○). Data were fit to eq 5. (B) pH profiles for k_{cat} with choline (●) and [1,2-$^2H_4$]choline (○). Data were fit to eq 5.

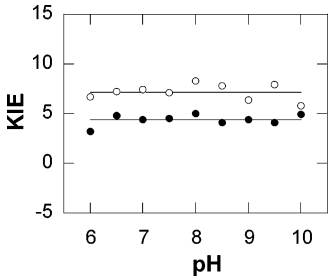

FIGURE 4: pH dependence of $^D(k_{cat}/K_m)$ (●) and $^D k_{cat}$ (○) values. CHO-E312D activity was measured at varying concentrations of choline or [1,2-$^2H_4$]choline under atmospheric oxygen conditions. The data for $^D k_{cat}$ and $^D(k_{cat}/K_m)$ were fit to $y = 7.1$ and $y = 4.4$, respectively.

a decrease in pH, consistent with the requirement of an unprotonated group in the reaction catalyzed by the Glu312Asp variant enzyme. An apparent pK_a value of 7.6 ± 0.04 was determined from the k_{cat}/K_m−pH profile. Substitution of choline with [1,2-$^2H_4$]choline did not result in changes in the apparent pK_a (7.6 ± 0.1) (Figure 3), suggesting that the value of 7.6 is likely a true thermodynamic pK_a value (*59*) that is not perturbed by kinetic commitments (*60*). In agreement with these conclusions, the resulting $^D(k_{cat}/K_m)$ value was pH-independent between pH 6 and 10 (Figure 4). The $^D k_{cat}$ value was also pH-independent and, interestingly, significantly larger than the $^D(k_{cat}/K_m)$ value, with average values of 7.1 ± 1.3 and 4.4 ± 1.2, respectively. These data suggest the presence of a pH-independent, internal equilibrium in the enzyme−substrate complex occurring prior to the cleavage of the substrate C−H bond (*60*).

The effects of solvent viscosity on the k_{cat}/K_m and k_{cat} values with choline as the substrate for CHO-E312D were determined at pH 10 to further probe for the presence of internal equilibria in the reductive half-reaction and the overall turnover of the enzyme, as previously reported for flavocytochrome b_2 (*61*). Initial rates of reaction were measured at varying concentrations of choline in air-saturated, 50 mM sodium pyrophosphate (pH 10) at 25 °C, in the presence of increasing amounts of glucose or sucrose as viscosigens. As shown in Figure 5, both the k_{cat}/K_m and k_{cat} values increased monotonically with an increase in the viscosity of the solvent, consistent with the presence of internal equilibria in both the reductive half-reaction and the overall turnover of the enzyme. Table 4 summarizes the effect of solvent viscosity on the k_{cat}/K_m and k_{cat} values for the Glu312Asp enzyme variant.

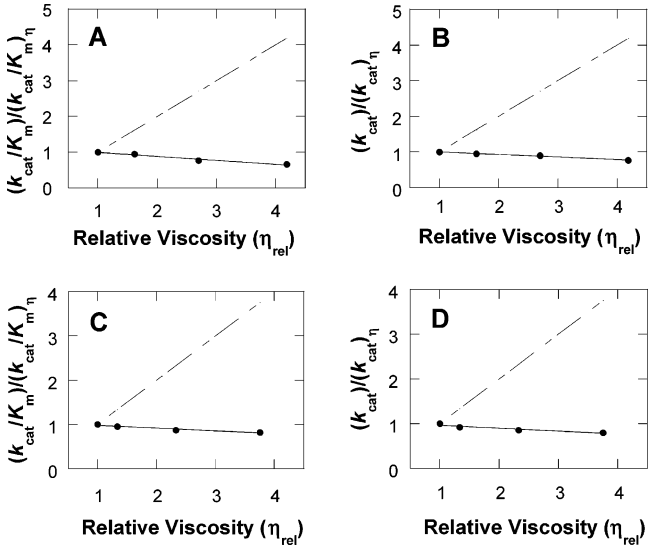

FIGURE 5: Effects of solvent viscosity on the k_{cat}/K_m and k_{cat} values with choline as the substrate for CHO-E312D with glucose or sucrose as the viscosigen at pH 10. (A) Normalized k_{cat}/K_m values as a function of relative solvent viscosity with glucose as the viscosigen. (B) Normalized k_{cat} values as a function of relative solvent viscosity with glucose as the viscosigen. (C) Normalized k_{cat}/K_m values as a function of relative solvent viscosity with sucrose as the viscosigen. (D) Normalized k_{cat} values as a function of relative solvent viscosity with sucrose as the viscosigen. Solid lines represent fits of the experimental data using eq 6. Dashed lines with a slope of 1 describe the hypothetical cases for fully diffusion-controlled reactions. The values of the relative viscosities of the reaction mixture at 25 °C were calculated according to the values at 20 °C from Lide (*46*). CHO-E312D activity was measured at varying concentrations of choline under atmospheric oxygen conditions.

Table 4: Effect of Solvent Viscosity on the Steady-State Kinetic Paramaters for CHO-E312D at pH 10

	viscosigen	viscosity effect[a]
k_{cat}/K_m (M^{-1} s^{-1})	glucose	-0.11 ± 0.02
k_{cat}/K_m (M^{-1} s^{-1})	sucrose	-0.06 ± 0.01
k_{cat} (s^{-1})	glucose	-0.07 ± 0.01
k_{cat} (s^{-1})	sucrose	-0.07 ± 0.02

[a] Viscosity effect values are relative to the values in the absence of viscosigen.

DISCUSSION

A detailed picture of the reaction mechanism of choline oxidase has emerged from previous pH and kinetic isotope effect studies (*16*, *17*, *58*), as well as mechanistic studies with substrate and product analogues (*6*, *19*, *22*), and site-directed mutants (*23*, *24*). The high-resolution structure of the wild-type enzyme reported in this study provides a structural framework within which previous mechanistic results can be further interpreted, as well as important information about residues that form the active site of choline oxidase. Furthermore, the mechanistic data presented for Glu312 enzyme variants shed light on the roles this residue plays in the binding and correct positioning of the alcohol substrate for the hydride transfer reaction of choline oxidation catalyzed by choline oxidase.

Mechanistic Insights from the Crystal Structure of Wild-Type Choline Oxidase. The active site of choline oxidase is formed by a cavity of approximately 125 Å^3 facing the *re* face of FAD, which is completely secluded from the exterior of the protein by a long loop region composed of residues 64−95. Whereas ∼60% of this loop is shielded from bulk solvent by the presence of the other subunit in the dimeric enzyme, residues 74−85 extend into the bulk solvent. This suggests that this portion of the loop may form a lid that allows entry of the substrate and exit of the reaction product to and from the active site. Similar loop regions that cover the active site have been observed previously in other members of the glucose-methanol-choline (GMC) oxidoreductase enzyme superfamily, such as glucose oxidase (*52*, *62*), pyranose 2-oxidase (*48*, *51*), cholesterol oxidase (*5*, *55*), and the flavin domain of cellobiose dehydrogenase (*50*). During catalysis in choline oxidase, opening and closing of the lid must necessarily follow the association of choline to form the catalytically relevant enzyme−substrate complex and precede the dissociation of glycine betaine from the enzyme−product complex.[4] The molecular mechanism underlying the entry and exit of organic ligands to and from the active site of choline oxidase, as well as in other members of the GMC superfamily, has not been investigated to date and represents an important question that can now be addressed.

As illustrated in Figure 2, the active site of choline oxidase is lined by both hydrophobic and hydrophilic residues playing important roles in both substrate binding and catalysis. The side chains of Trp61, Trp331, and Phe357 form a hydrophobic cage on the active site surface that is adjacent to the isoalloxazine ring of the flavin. These residues and the negatively charged side chain of Glu312 constitute the site of interaction for binding the trimethylammoniun moiety of choline via cation-π and electrostatic interactions. The importance of the negative charge at position 312 for substrate binding is demonstrated by the ∼500-fold increase in the K_d value for choline binding determined by anaerobic stopped-flow spectrophotometry in the E312Q mutant. Since glutamine is isosteric with glutamate, one can assume similar active site structures and binding modes of choline in the E312Q mutant and wild-type enzymes. This supports an energetic contribution of ∼15 kJ/mol to be estimated for the ionic interaction of the negative charge at position 312 and the positive charge of choline. Moreover, this value agrees well with the value of ∼13 kJ/mol that was recently estimated from mechanistic studies on choline oxidase with the choline analogue devoid of positive charge, 3,3-dimethylbutan-1-ol (*22*). An aromatic cage structurally surrounding a negatively charged amino acid residue also appears to be a common feature in enzymes and proteins that bind ligands containing trimethylammoniun groups. For example, similar binding motifs are observed in phospholipase C (*63*), acetylcholinesterase (*64*−*66*), CTP:phosphocholine cytidylyltransferase (*67*), and the periplasmic ligand-binding proteins pro-X and Opu-C (*68*−*70*).

[4] It is assumed here that the lid topping the active site cavity is closed not only in the enzyme devoid of ligands, as observed in this study, but also when the enzyme is in complex with the substrate, as reported previously for another member of the GMC oxidoreductase superfamily, cholesterol oxidase (*4*, *5*). This assumption is based on the observation that, upon docking of choline in the active site of the enzyme, all the residues proposed to participate in substrate binding and catalysis appear to be spatially positioned in a fashion that is consistent with all the available mechanistic and biochemical data. A closed lid configuration during enzymatic turnover is also consistent with earlier kinetic data showing that the betaine aldehyde intermediate predominantly remains bound at the active site during turnover with choline (*6*).

Scheme 2: Chemical Mechanism for the Oxidation of Choline to Betaine Aldehyde Catalyzed by Choline Oxidase

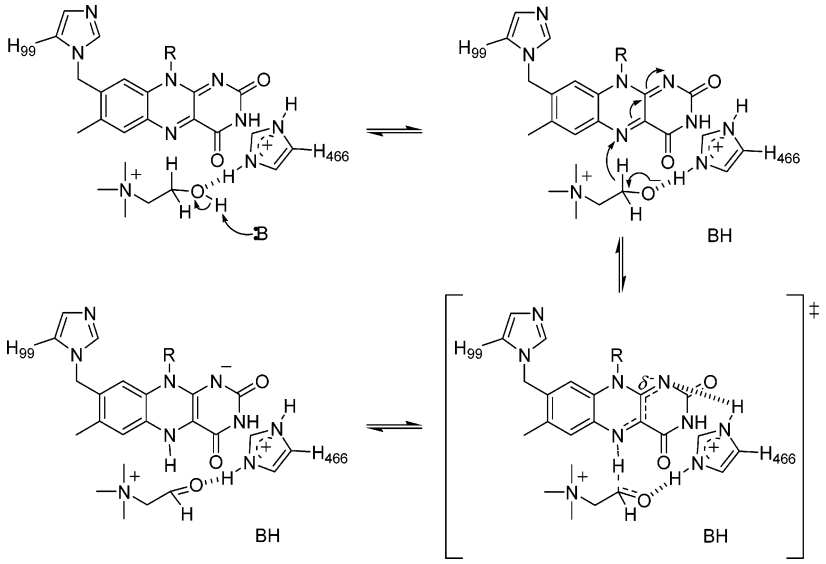

Previous mechanistic studies have established that the oxidation of choline catalyzed by choline oxidase occurs through a highly asynchronous chemical mechanism. The formation of a choline alkoxide species precedes the hydride transfer reaction from this activated substrate to the enzyme-bound flavin (Scheme 2) (*16*). A group with a thermodynamic pK_a of 7.5 has been proposed to be responsible for the abstraction of the hydroxyl H^+ from the substrate (*16*, *17*, *58*). The structure of choline oxidase indicates that Glu312, His351, and His466 are the only residues lining the active site cavity of the enzyme with the ability to act as a general base. The side chain of Glu312 can be immediately ruled out as being responsible for choline activation because it is ~8 Å from the N5 atom of FAD, a distance that is too long for such a catalytic role. In agreement with this conclusion, site-directed mutagenesis data presented here for enzyme variants containing glutamine or aspartate at position 312 are consistent with Glu312 participating in substrate binding (vide infra). Recently published mechanistic data for mutant forms of choline oxidase in which His466 has been replaced by other amino acids strongly suggest that this residue is likely not the group responsible for the removal of the hydroxyl H^+ of choline. Rather, those results point out that His466 is protonated during the reductive half-reaction in which choline is oxidized by choline oxidase (Scheme 2) (*23*, *24*). Indeed, with the His466Ala mutant enzyme, the activity could be partially rescued with imidazolium, but not imidazole (*23*), and both the k_{cat}− and k_{cat}/K_m−pH profiles still showed the requirement for a catalytic base (*23*). Furthermore, the His466Asp enzyme was completely devoid of enzymatic activity with choline, under catalytic turnover or anaerobic conditions (*24*). Thus, on the basis of the structural information now available, it appears that His351 may serve as the general base in the oxidation reaction catalyzed by choline oxidase. This hypothesis is currently under study with the characterization of mutant variants of choline oxidase in which His351 has been replaced with amino acids carrying other functional groups.

Recently published mechanistic data have established that in choline oxidase the hydride transfer reaction occurs within a highly preorganized enzyme−substrate complex (*21*), by exploiting the mechanical effects that result in the tunneling of the hydride ion from the α-carbon of the choline alkoxide to the flavin N5 atom (*20*) (Scheme 2). This, in turn, requires minimal independent movement of the activated choline alkoxide relative to the isoalloxazine ring of the flavin. Consequently, only dynamic motions in the activated enzyme−substrate complex that promote the hydride transfer reaction are permitted. The active site cavity of choline oxidase, which has a volume slightly larger than that of choline, as well as the location of the groups involved in substrate binding and catalysis is fully consistent with this mechanistic hypothesis (Figure 2). Indeed, the isoalloxazine ring of the cofactor, which acts as hydride acceptor in the oxidation reaction, is physically constrained by the covalent linkage of the FAD C8M atom with His99, the proximity of Ile103 to the pyrimidine ring, and several contacts with the backbone atoms between His99 and Ile103. To a similar extent, the choline alkoxide species that donates the hydride in the oxidation reaction is physically constrained by electrostatic interactions of its positively charged trimethylammonium group with Glu312 at one extremity and its negatively charged alkoxide O atom with the positively charged side chain of His466 at the opposite end (*23*, *24*).

Mechanistic Insights into the Role of Glu312 in Choline Oxidase. The mutant form of choline oxidase in which Glu312 has been replaced with aspartate is properly folded and functional, as suggested by the steady-state and rapid kinetic data presented in this study. The E312D enzyme variant exhibited the same sequential steady-state kinetic mechanism of reaction as the wild-type enzyme. Moreover, pH profiles of the k_{cat}/K_m values for choline or [1,2-$^2H_4$]-choline as substrates for the E312D variant identified a pK_a value of ~7.5 for the general base that activates choline in catalysis, which is similar to the value previously reported for the wild-type enzyme (*17*, *58*). Finally, both the $^Dk_{red}$ and K_d values with choline as the substrate for CHO-E312D were not significantly different from those of the wild-type enzyme. Consequently, the comparison of the mechanistic properties of the Glu312Asp and wild-type enzymes could provide direct evidence of the importance of spatial location of the negative charge on residue 312 in the reaction catalyzed by choline oxidase.

The spatial location of the negative charge on residue 312 is important for the oxidation of the alcohol substrate, but not for the following oxidation of the enzyme-bound reduced flavin. This conclusion is supported by the 30-fold decrease in the k_{cat}/K_m value for choline and the lack of significant changes in the k_{cat}/K_m value for oxygen observed with the Glu312Asp enzyme variant as compared to the values of the wild-type enzyme determined at pH 10. The lack of involvement of Glu312 in the oxidative half-reaction is in agreement with previous pH profile data for the wild-type enzyme (*17*, *58*), showing that no ionizable groups with pK_a values between 6 and 10 participate in the oxidation of the reduced flavin.

Substitution of Glu312 with an aspartate residue significantly affects the hydride transfer reaction that results in the reduction of the flavin cofactor but has little if any effect on the binding of the substrate in the active site of the enzyme. Evidence supporting this conclusion comes from anaerobic substrate reduction experiments using a stopped-flow spectrophotometer, showing that in the Glu312Asp enzyme the k_{red} value at pH 10 is 260 times lower than in the wild-type enzyme, whereas the K_d value is not significantly changed. In the wild-type form of choline oxidase (*20*), the hydride ion tunnels from the α-carbon of the activated substrate to the enzyme-bound flavin N5 atom, with little independent movement of the hydride donor and acceptor, other than those conducive to tunneling of the hydride ion. Due to the larger distance between the donor and acceptor of the hydride ion that necessarily arises from the E312D mutation, assuming similar overall structures, one can speculate that the mode of hydride ion transfer in the Glu312Asp mutant enzyme may be significantly altered with respect to that of the wild-type enzyme. In this respect, the large deuterium kinetic isotope effect determined here for the Glu312Asp mutant enzyme, with a $^{D}k_{red}$ value of ∼9, bodes well as an essential prerequisite for future mechanistic studies aimed at investigating the mode of hydride ion transfer in the Glu312Asp enzyme.

The thermodynamic pK_a of ∼7.5 for the group that acts as a general base in the oxidation of choline is not affected by the substitution of Glu312 with an aspartate residue, as suggested by the comparison of the mechanistic data presented here for CHO-E312D and previously published data for the wild-type enzyme (*17*, *58*). Evidence for the value of ∼7.5 determined in the k_{cat}/K_m−pH profile with CHO-E312D being a thermodynamic pK_a value comes from kinetic isotope effect data, showing that the $^{D}(k_{cat}/K_m)$ value is pH-independent between pH 6 and 10. This is consistent with lack of external commitments to catalysis in the mutant enzyme, which would perturb the observed kinetic pK_a value from its thermodynamic value (*59*). The observation that the same pK_a value is seen in the k_{cat}/K_m−pH profiles with choline and [1,2-$^2H_4$]choline provides independent support for the observed pK_a being a thermodynamic value. Indeed, a value significantly lower than 7.5 would be expected with a slower substrate such as [1,2-$^2H_4$]choline, for which C−D bond cleavage is at least 4 times slower than C−H bond cleavage in the reductive half-reaction (*71*).

Upon substitution of Glu312 with aspartate, the enzyme−substrate Michaelis complex undergoes a kinetically relevant, pH-independent, isomerization prior to the hydride ion transfer reaction. Evidence supporting this conclusion comes from the effects of solvent viscosity on the k_{cat}/K_m value with choline as the substrate for CHO-E312D. Indeed, the normalized k_{cat}/K_m values decreased monotonically with an increase in the relative viscosity of the solvent, irrespective of the use of glucose or sucrose as the solvent viscosigen. These data cannot be explained with solvent viscosity reporting on the contribution of substrate binding steps on the overall rate for the reductive half-reaction in which choline is oxidized to betaine aldehyde, for which normalized k_{cat}/K_m values are expected not to change or to increase to various extents with an increase in relative viscosity (*72*−*75*). In contrast, the effects of solvent viscosity observed with CHO-E312D can be readily explained by the presence of a conformational change in the enzyme−substrate complex that is sensitive to the viscosity of the solvent. Independent evidence for the presence of a kinetically relevant conformational change in the enzyme−substrate complex comes from kinetic isotope effects on the k_{cat}/K_m value with choline as the substrate for CHO-E312D, showing pH-independent $^{D}(k_{cat}/K_m)$ values significantly lower than the $^{D}k_{cat}$ values. It is well-established that kinetic isotope effects determined using the steady-state kinetic approach may be significantly lower than their intrinsic values in the presence of commitments to catalysis (*60*). In choline oxidase, both the external forward commitment to catalysis and the reverse commitment to catalysis are pH-dependent, since they both include the chemical step in which the hydroxyl proton is abstracted from the alcohol substrate. However, these commitments to catalysis can be immediately ruled out as being responsible for lowering the observed $^{D}(k_{cat}/K_m)$ value because both the pH independence of the $^{D}(k_{cat}/K_m)$ values and the similarity in the pK_a values of ∼7.5 determined from the pH profiles of the k_{cat}/K_m values with choline and [1,2-$^2H_4$]choline argue against the presence of pH-dependent commitments to catalysis (*60*, *76*, *77*). Consequently, any decrease in the observed $^{D}(k_{cat}/K_m)$ values seen with CHO-E312D must necessarily arise from a pH-independent, internal equilibrium involving the enzyme−substrate complex. In this regard, an internal equilibrium of the type described here has been recently proposed for the wild-type form of choline oxidase from the comparison of the effects of pH and temperature on the kinetic isotope effects in reversible and irreversible catalytic regimes (*21*). It is attractive to hypothesize that the protein conformational change that is associated with the internal equilibrium in the enzyme−substrate complex may be triggered by the deprotonation of the alcohol substrate that yields the alkoxide species, which was previously demonstrated to occur prior to the subsequent hydride transfer reaction (*16*).

Conclusions. The results of the crystallographic and mechanistic investigations presented in this study demonstrate the important role of Glu312 in the binding and positioning of the alcohol substrate for catalysis in choline oxidase. The negative charge on residue 312 is involved in an electrostatic interaction with the positive charge of choline that anchors the nonreactive end of the substrate in the active site of the enzyme. Thus, the spatial location of the negative charge in the active site is important for the correct positioning of the substrate for the hydride transfer reaction from the activated choline alkoxide to the flavin N5 atom. Moreover, the crystal structure of choline oxidase provides detailed structural information that correlates well with all

the mechanistic information that is currently available on the enzyme. It shows that the active site of choline oxidase is well-suited to maximizing several aspects of the reaction. For example, productive binding of choline (a) positions the catalytic base appropriately to activate the substrate, (b) places the activated alkoxide species for maximum stabilization by a nearby positive charge, and (c) places the α CH group near the flavin N5 moiety of the isoalloxazine ring. Together, all these features efficiently position the substrate for the hydride transfer reaction within a highly preorganized enzyme−substrate complex. Finally, the availability of the three-dimensional structure of the enzyme represents an essential prerequisite for future mechanistic studies aimed at establishing the contribution of selected active site residues that do not participate directly in catalysis, e.g., Glu312, toward hydride transfer and tunneling in the oxidation of the alcohol substrate catalyzed by flavin-dependent enzymes.

ACKNOWLEDGMENT

X-ray diffraction data were collected at Southeast Regional Collaborative Access Team (SER-CAT) beamlines 22-ID and 22-BM at the Advanced Photon Source, Argonne National Laboratory (SER-CAT supporting institutions may be found at www.ser-cat.org/members.html). Use of the Advanced Photon Source was supported by the U.S. Department of Energy, Office of Science, Office of Basic Energy Sciences, under Contract W-31-109-Eng-38. We thank the SER-CAT staff at APS for assistance during data collection and Dr. Zhongmin Jin for assistance with the mail-in crystallography program. We acknowledge the efforts of Megan O'Neill during the initial crystallization trials of choline oxidase.

SUPPORTING INFORMATION AVAILABLE

Structure-based sequence alignment with homologues of choline oxidase with known X-ray structures (Figure S1), UV−visible absorbance spectra of a mixture of flavin semiquinone and oxidized and fully oxidized FAD for CHO-E312A (Figure S2), rate of flavin reduction in CHO-E312Q as a function of choline or [1,2-$^2H_4$]choline concentration (Figure S3), estimation of K_m for oxygen in CHO-E312D at pH 5 and 10 (Figure S4), rate of flavin reduction in CHO-E312D as a function of choline or [1,2-$^2H_4$]choline concentration (Figure S5), quantitative structural similarity between choline oxidase and selected homologues (Table S1), kinetic parameters and kinetic isotope effect for CHO-E312D between pH 5 and 10 (Table S2), and solvent viscosity effects on steady-state kinetic parameters for CHO-E312D with choline as the substrate, and glucose and sucrose as viscosigens (Table S3). This material is available free of charge via the Internet at http://pubs.acs.org.

REFERENCES

1. Dixon, D. A., Lindner, D. L., Branchaud, B., and Lipscomb, W. N. (1979) Conformations and electronic structures of oxidized and reduced isoalloxazine, *Biochemistry 18*, 5770−5775.
2. Lennon, B. W., Williams, C. H., Jr., and Ludwig, M. L. (1999) Crystal structure of reduced thioredoxin reductase from *Escherichia coli*: Structural flexibility in the isoalloxazine ring of the flavin adenine dinucleotide cofactor, *Protein Sci. 8*, 2366−2379.
3. Sheng, D., Ballou, D. P., and Massey, V. (2001) Mechanistic studies of cyclohexanone monooxygenase: Chemical properties of intermediates involved in catalysis, *Biochemistry 40*, 11156−11167.
4. Lario, P. I., Sampson, N., and Vrielink, A. (2003) Sub-atomic resolution crystal structure of cholesterol oxidase: What atomic resolution crystallography reveals about enzyme mechanism and the role of the FAD cofactor in redox activity, *J. Mol. Biol. 326*, 1635−1650.
5. Li, J., Vrielink, A., Brick, P., and Blow, D. M. (1993) Crystal structure of cholesterol oxidase complexed with a steroid substrate: Implications for flavin adenine dinucleotide dependent alcohol oxidases, *Biochemistry 32*, 11507−11515.
6. Fan, F., Germann, M. W., and Gadda, G. (2006) Mechanistic studies of choline oxidase with betaine aldehyde and its isosteric analogue 3,3-dimethylbutyraldehyde, *Biochemistry 45*, 1979−1986.
7. Bae, J. H., Anderson, S. H., and Miller, K. J. (1993) Identification of a high-affinity glycine betaine transport system in *Staphylococcus aureus*, *Appl. Environ. Microbiol. 59*, 2734−2736.
8. Pichereau, V., Bourot, S., Flahaut, S., Blanco, C., Auffray, Y., and Bernard, T. (1999) The osmoprotectant glycine betaine inhibits salt-induced cross-tolerance towards lethal treatment in *Enterococcus faecalis*, *Microbiology 145* (Part 2), 427−435.
9. Chen, T. H., and Murata, N. (2002) Enhancement of tolerance of abiotic stress by metabolic engineering of betaines and other compatible solutes, *Curr. Opin. Plant Biol. 5*, 250−257.
10. Rontein, D., Basset, G., and Hanson, A. D. (2002) Metabolic engineering of osmoprotectant accumulation in plants, *Metab. Eng. 4*, 49−56.
11. Sanchez-Aguayo, I., Rodriguez-Galan, J. M., Garcia, R., Torreblanca, J., and Pardo, J. M. (2004) Salt stress enhances xylem development and expression of S-adenosyl-L-methionine synthase in lignifying tissues of tomato plants, *Planta 220*, 278−285.
12. Shirasawa, K., Takabe, T., Takabe, T., and Kishitani, S. (2006) Accumulation of glycinebetaine in rice plants that overexpress choline monooxygenase from spinach and evaluation of their tolerance to abiotic stress, *Ann. Bot. (Oxford, U.K.) 98*, 565−571.
13. Waditee, R., Bhuiyan, M. N., Rai, V., Aoki, K., Tanaka, Y., Hibino, T., Suzuki, S., Takano, J., Jagendorf, A. T., Takabe, T., and Takabe, T. (2005) Genes for direct methylation of glycine provide high levels of glycinebetaine and abiotic-stress tolerance in *Synechococcus* and *Arabidopsis*, *Proc. Natl. Acad. Sci. U.S.A. 102*, 1318−1323.
14. O'Callaghan, J., and Condon, S. (2000) Growth of *Lactococcus lactis* strains at low water activity: Correlation with the ability to accumulate glycine betaine, *Int. J. Food Microbiol. 55*, 127−131.
15. Velasco-Garcia, R., Chacon-Aguilar, V. M., Hervert-Hernandez, D., and Munoz-Clares, R. A. (2003) Inactivation of betaine aldehyde dehydrogenase from *Pseudomonas aeruginosa* and *Amaranthus hypochondriacus* L. leaves by disulfiram, *Chem.-Biol. Interact. 143−144*, 149−158.
16. Fan, F., and Gadda, G. (2005) On the catalytic mechanism of choline oxidase, *J. Am. Chem. Soc. 127*, 2067−2074.
17. Gadda, G. (2003) pH and deuterium kinetic isotope effects studies on the oxidation of choline to betaine-aldehyde catalyzed by choline oxidase, *Biochim. Biophys. Acta 1650*, 4−9.
18. Gadda, G., and McAllister-Wilkins, E. E. (2003) Cloning, expression, and purification of choline dehydrogenase from the moderate halophile *Halomonas elongata*, *Appl. Environ. Microbiol. 69*, 2126−2132.
19. Gadda, G., Powell, N. L., and Menon, P. (2004) The trimethylammonium headgroup of choline is a major determinant for substrate binding and specificity in choline oxidase, *Arch. Biochem. Biophys. 430*, 264−273.
20. Fan, F., and Gadda, G. (2005) Oxygen- and temperature-dependent kinetic isotope effects in choline oxidase: Correlating reversible hydride transfer with environmentally enhanced tunneling, *J. Am. Chem. Soc. 127*, 17954−17961.
21. Fan, F., and Gadda, G. (2007) An internal equilibrium preorganizes the enzyme-substrate complex for hydride tunneling in choline oxidase, *Biochemistry 46*, 6402−6408.
22. Gadda, G., Fan, F., and Hoang, J. V. (2006) On the contribution of the positively charged headgroup of choline to substrate binding and catalysis in the reaction catalyzed by choline oxidase, *Arch. Biochem. Biophys. 451*, 182−187.
23. Ghanem, M., and Gadda, G. (2005) On the catalytic role of the conserved active site residue His466 of choline oxidase, *Biochemistry 44*, 893−904.

24. Ghanem, M., and Gadda, G. (2006) Effects of reversing the protein positive charge in the proximity of the flavin N(1) locus of choline oxidase, *Biochemistry 45*, 3437−3447.
25. Pudney, C. R., Hay, S., Sutcliffe, M. J., and Scrutton, N. S. (2006) Alpha-secondary isotope effects as probes of "tunneling-ready" configurations in enzymatic H-tunneling: Insight from environmentally coupled tunneling models, *J. Am. Chem. Soc. 128*, 14053−14058.
26. Rajagopalan, P. T., and Benkovic, S. J. (2002) Preorganization and protein dynamics in enzyme catalysis, *Chem. Rec. 2*, 24−36.
27. Fan, F., Ghanem, M., and Gadda, G. (2004) Cloning, sequence analysis, and purification of choline oxidase from *Arthrobacter globiformis*: A bacterial enzyme involved in osmotic stress tolerance, *Arch. Biochem. Biophys. 421*, 149−158.
28. Holyoak, T., Fenn, T. D., Wilson, M. A., Moulin, A. G., Ringe, D., and Petsko, G. A. (2003) Malonate: A versatile cryoprotectant and stabilizing solution for salt-grown macromolecular crystals, *Acta Crystallogr. D59*, 2356−2358.
29. Otwinowski, Z., and Minor, W. (1997) Processing the X-ray diffraction data collected in oscillation mode, *Methods Enzymol. 276*, 307−326.
30. Kantardjieff, K. A., and Rupp, B. (2003) Matthews coefficient probabilities: Improved estimates for unit cell contents of proteins, DNA, and protein-nucleic acid complex crystals, *Protein Sci. 12*, 1865−1871.
31. Matthews, B. W. (1968) Solvent content of protein crystals, *J. Mol. Biol. 33*, 491−497.
32. Vagin, A. A., and Teplyakov, A. (1997) MOLREP: an Automated Program for Molecular Replacement, *J. Appl. Crystallogr. 20*, 1022−1025.
33. Collaborative Computational Project, Number 4 (1994) The CCP4 Suite: Programs for Protein Crystallography, *Acta Cryst. D50*, 760−763.
34. Wohlfahrt, G., Witt, S., Hendle, J., Schomburg, D., Kalisz, H. M., and Hecht, H. J. (1999) 1.8 and 1.9 Å resolution structures of the *Penicillium amagasakiense* and *Aspergillus niger* glucose oxidases as a basis for modelling substrate complexes, *Acta Crystallogr. 55*, 969−977.
35. Brünger, A. T., Adams, P. D., Clore, G. M., DeLano, W. L., Gros, P., Grosse-Kunstleve, R. W., Jiang, J. S., Kuszewski, J., Nilges, M., Pannu, N. S., Read, R. J., Rice, L. M., Simonson, T., and Warren, G. L. (1998) Crystallography & NMR system: A new software suite for macromolecular structure determination, *Acta Crystallogr. D54*, 905−921.
36. Terwilliger, T. C. (2004) Using prime-and-switch phasing to reduce model bias in molecular replacement, *Acta Crystallogr. D60*, 6.
37. Terwilliger, T. C. (2003) SOLVE and RESOLVE: Automated structure solution and density modification, *Methods Enzymol. 374*, 22−37.
38. Kleywegt, G. J., and Jones, T. A. (1997) Model building and refinement practice, *Methods Enzymol. 277*, 208−230.
39. Pannu, N. S., Murshudov, G. N., Dodson, E. J., and Read, R. J. (1998) Incorporation of prior phase information strengthens maximum-likelihood structure refinement, *Acta Crystallogr. D54*, 1285−1294.
40. Read, R. J. (1997) Model phases: Probabilities and bias, *Methods Enzymol. 277*, 110−128.
41. van Aalten, D. M., Bywater, R., Findlay, J. B., Hendlich, M., Hooft, R. W., and Vriend, G. (1996) PRODRG, a program for generating molecular topologies and unique molecular descriptors from coordinates of small molecules, *J. Comput.-Aided Mol. Des. 10*, 255−262.
42. Lamzin, V. S., and Wilson, K. S. (1993) Automated refinement of protein models, *Acta Crystallogr. D49*, 129−147.
43. Laskowski, R. A., Moss, D. S., and Thornton, J. M. (1993) Main-chain bond lengths and bond angles in protein structures, *J. Mol. Biol. 231*, 1049−1067.
44. Morris, A. L., MacArthur, M. W., Hutchinson, E. G., and Thornton, J. M. (1992) Stereochemical quality of protein structure coordinates, *Proteins 12*, 345−364.
45. Kabsch, W., and Sander, C. (1983) Dictionary of protein secondary structure: Pattern recognition of hydrogen-bonded and geometrical features, *Biopolymers 22*, 2577−2637.
46. Lide, D. R. (2000) in *Handbook of Chemistry and Physics*, pp 8−57, CRC Press, Boca Raton, FL.
47. Albrecht, M., and Lengauer, T. (2003) Pyranose oxidase identified as a member of the GMC oxidoreductase family, *Bioinformatics 19*, 1216−1220.
48. Bannwarth, M., Bastian, S., Heckmann-Pohl, D., Giffhorn, F., and Schulz, G. E. (2004) Crystal structure of pyranose 2-oxidase from the white-rot fungus *Peniophora* sp., *Biochemistry 43*, 11683−11690.
49. Cavener, D. R. (1992) GMC oxidoreductases. A newly defined family of homologous proteins with diverse catalytic activities, *J. Mol. Biol. 223*, 811−814.
50. Hallberg, B. M., Henriksson, G., Pettersson, G., and Divne, C. (2002) Crystal structure of the flavoprotein domain of the extracellular flavocytochrome cellobiose dehydrogenase, *J. Mol. Biol. 315*, 421−434.
51. Hallberg, B. M., Leitner, C., Haltrich, D., and Divne, C. (2004) Crystal structure of the 270 kDa homotetrameric lignin-degrading enzyme pyranose 2-oxidase, *J. Mol. Biol. 341*, 781−796.
52. Hecht, H. J., Kalisz, H. M., Hendle, J., Schmid, R. D., and Schomburg, D. (1993) Crystal structure of glucose oxidase from *Aspergillus niger* refined at 2.3 Å resolution, *J. Mol. Biol. 229*, 153−172.
53. Henriksson, G., Johansson, G., and Pettersson, G. (2000) A critical review of cellobiose dehydrogenases, *J. Biotechnol. 78*, 93−113.
54. Kiess, M., Hecht, H. J., and Kalisz, H. M. (1998) Glucose oxidase from *Penicillium amagasakiense*. Primary structure and comparison with other glucose-methanol-choline (GMC) oxidoreductases, *Eur. J. Biochem. 252*, 90−99.
55. Yue, Q. K., Kass, I. J., Sampson, N. S., and Vrielink, A. (1999) Crystal structure determination of cholesterol oxidase from *Streptomyces* and structural characterization of key active site mutants, *Biochemistry 38*, 4277−4286.
56. Fraaije, M. W., and Mattevi, A. (2000) Flavoenzymes: Diverse catalysts with recurrent features, *Trends Biochem. Sci. 25*, 126−132.
57. Rand, T., Halkier, T., and Hansen, O. C. (2003) Structural characterization and mapping of the covalently linked FAD cofactor in choline oxidase from *Arthrobacter globiformis*, *Biochemistry 42*, 7188−7194.
58. Ghanem, M., Fan, F., Francis, K., and Gadda, G. (2003) Spectroscopic and kinetic properties of recombinant choline oxidase from *Arthrobacter globiformis*, *Biochemistry 42*, 15179−15188.
59. Cook, P. F., Blanchard, J. S., and Cleland, W. W. (1980) Primary and secondary deuterium isotope effects on equilibrium constants for enzyme-catalyzed reactions, *Biochemistry 19*, 4853−4858.
60. Cleland, W. W. (1982) The use of isotope effects to determine transition-state structure for enzymic reactions, *Methods Enzymol. 87*, 625−641.
61. Sobrado, P., and Fitzpatrick, P. F. (2003) Solvent and primary deuterium isotope effects show that lactate CH and OH bond cleavages are concerted in Y254F flavocytochrome b2, consistent with a hydride transfer mechanism, *Biochemistry 42*, 15208−15214.
62. Hecht, H. J., Schomburg, D., Kalisz, H., and Schmid, R. D. (1993) The 3D structure of glucose oxidase from *Aspergillus niger*. Implications for the use of GOD as a biosensor enzyme, *Biosens. Bioelectron. 8*, 197−203.
63. Martin, S. F., Follows, B. C., Hergenrother, P. J., and Trotter, B. K. (2000) The choline binding site of phospholipase C (*Bacillus cereus*): Insights into substrate specificity, *Biochemistry 39*, 3410−3415.
64. Pomponi, M., Sacchi, S., Colella, A., Patamia, M., and Marta, M. (1998) The role of TRP84 in catalytic power and the specificity of AChE, *Biophys. Chem. 72*, 239−246.
65. Gasch, A. P., Spellman, P. T., Kao, C. M., Carmel-Harel, O., Eisen, M. B., Storz, G., Botstein, D., and Brown, P. O. (2000) Genomic expression programs in the response of yeast cells to environmental changes, *Mol. Biol. Cell 11*, 4241−4257.
66. Harel, M., Kryger, G., Rosenberry, T. L., Mallender, W. D., Lewis, T., Fletcher, R. J., Guss, J. M., Silman, I., and Sussman, J. L. (2000) Three-dimensional structures of *Drosophila melanogaster* acetylcholinesterase and of its complexes with two potent inhibitors, *Protein Sci. 9*, 1063−1072.
67. Kwak, B. Y., Zhang, Y. M., Yun, M., Heath, R. J., Rock, C. O., Jackowski, S., and Park, H. W. (2002) Structure and mechanism of CTP:phosphocholine cytidylyltransferase (LicC) from *Streptococcus pneumoniae*, *J. Biol. Chem. 277*, 4343−4350.
68. Horn, C., Sohn-Bosser, L., Breed, J., Welte, W., Schmitt, L., and Bremer, E. (2006) Molecular determinants for substrate specificity of the ligand-binding protein OpuAC from *Bacillus subtilis* for the compatible solutes glycine betaine and proline betaine, *J. Mol. Biol. 357*, 592−606.

69. Schiefner, A., Breed, J., Bosser, L., Kneip, S., Gade, J., Holtmann, G., Diederichs, K., Welte, W., and Bremer, E. (2004) Cation-π interactions as determinants for binding of the compatible solutes glycine betaine and proline betaine by the periplasmic ligand-binding protein ProX from *Escherichia coli*, *J. Biol. Chem. 279*, 5588−5596.
70. Schiefner, A., Holtmann, G., Diederichs, K., Welte, W., and Bremer, E. (2004) Structural basis for the binding of compatible solutes by ProX from the hyperthermophilic archaeon *Archaeoglobus fulgidus*, *J. Biol. Chem. 279*, 48270−48281.
71. Cleland, W. W. (1982) The use of pH studies to determine chemical mechanisms of enzyme-catalyzed reactions, *Methods Enzymol. 87*, 390−405.
72. Agmon, N. (1985) A diffusion Michaelis-Menten mechanism: Continuous conformational change in enzymatic kinetics, *J. Theor. Biol. 113*, 711−717.
73. Sobrado, P., Daubner, S. C., and Fitzpatrick, P. F. (2001) Probing the relative timing of hydrogen abstraction steps in the flavocytochrome b2 reaction with primary and solvent deuterium isotope effects and mutant enzymes, *Biochemistry 40*, 994−1001.
74. Somogyi, B., Norman, J. A., Zempel, L., and Rosenberg, A. (1988) Viscosity and transient solvent accessibility of Trp-63 in the native conformation of lysozyme, *Biophys. Chem. 32*, 1−13.
75. Su, Q., and Klinman, J. P. (1999) Nature of oxygen activation in glucose oxidase from *Aspergillus niger*: The importance of electrostatic stabilization in superoxide formation, *Biochemistry 38*, 8572−8581.
76. Emanuele, J. J., and Fitzpatrick, P. F. (1995) Mechanistic studies of the flavoprotein tryptophan 2-monooxygenase. 1. Kinetic mechanism, *Biochemistry 34*, 3710−3715.
77. Grissom, C. B., and Cleland, W. W. (1988) Isotope effect studies of the chemical mechanism of pig heart NADP isocitrate dehydrogenase, *Biochemistry 27*, 2934−2943.
78. Bradford, M. M. (1976) A rapid and sensitive method for the quantitation of microgram quantities of protein utilizing the principle of protein-dye binding, *Anal. Biochem. 72*, 248−254.

BI7017943